

Raman spectra and DFT calculations for botryococcene and methylsqualene hydrocarbons from the B race of the green microalga *Botryococcus braunii*



Mehmet Tatli ^a, Hye Jin Chun ^b, Charles H. Camp Jr. ^c, Jingting Li ^d, Marcus T. Cicerone ^c, Wei-Chuan Shih ^{d,e,f,g}, Jaan Laane ^b, Timothy P. Devarenne ^{a,*}

^a Department of Biochemistry & Biophysics, Texas A&M University, College Station, TX, United States

^b Department of Chemistry, Texas A&M University, College Station, TX, United States

^c Biosystems and Biomaterials Division, National Institute of Standards and Technology, Gaithersburg, MD, United States

^d Department of Electrical and Computer Engineering, University of Houston, Houston, TX, United States

^e Department of Biomedical Engineering, University of Houston, Houston, TX, United States

^f Department of Chemistry, University of Houston, Houston, TX, United States

^g Program of Materials Science and Engineering, University of Houston, Houston, TX, United States

ARTICLE INFO

Article history:

Received 1 May 2017

Accepted 28 June 2017

Available online 30 June 2017

Keywords:

Botryococcus braunii

Botryococcene

DFT calculations

Methylsqualene

Raman spectroscopy

Triterpenoids

ABSTRACT

Botryococcus braunii, a green colonial microalga, is a prodigious producer of liquid hydrocarbon oils that can be used as renewable feedstocks for producing combustion engine fuels. The B race of *B. braunii* mainly produces the triterpene hydrocarbons known as botryococcenes, which have over twenty known structures. Minor hydrocarbons in the B race include the triterpene methylsqualenes. Here we report an examination of the molecular structure for ten botryococcenes and five methylsqualenes using Raman spectroscopy and density functional theory (DFT) calculations in an effort to distinguish between these structurally similar molecules by spectroscopic approaches. The DFT calculations show that these molecules have between 243 and 271 vibrational frequencies. A comparison of the experimental Raman spectroscopy and DFT calculations indicates several spectral regions such as those for $\nu(\text{C}=\text{C})$ stretching, CH_2/CH_3 bending, and ring bending can be used to distinguish between these molecules. In an extension of this analysis, a broadband coherent anti-Stokes Raman spectroscopy (BCARS) analysis was used to clearly distinguish between several botryococcenes isomers.

© 2017 Elsevier B.V. All rights reserved.

1. Introduction

Algae produced lipids are considered a potential renewable feedstock source to replace petroleum-based transportation fuels in order to address concerns over global climate changes due to fossil fuel derived greenhouse gas build up [1]. One alga that produces large amounts of lipids in the form of liquid hydrocarbons is the green colony-forming microalga *Botryococcus braunii* [2]. Hydrocarbons produced by *B. braunii* have been identified as major constituents of currently used petroleum and coal deposits indicating contribution by this organism to the formation of these deposits over geologic time [3–7]. Thus, these *B. braunii* hydrocarbons can be converted into combustion engine fuels using

conventional petroleum hydrocracking procedures [8–10].

B. braunii is divided into three chemical races, A, B, and L, that are defined by the type of hydrocarbon produced [2]. The B race of *B. braunii*, the focus of this study, produces 30–40% of its dry weight as hydrocarbons in the form of two types of isoprenoid triterpenes; botryococcenes as the major accumulating hydrocarbons, and methylated squalenes as minor hydrocarbon components [2]. Botryococcenes and squalenes follow a very similar biosynthetic route and thus are very similar in structure with the exception of an ethene branch in the middle of the botryococcene structure that is not present in squalenes (Fig. 1). Both botryococcenes and methylated squalenes start as C_{30} molecules, which are methylated at carbons 3, 7, 16, and 20 for botryococcenes and carbons 3, 7, 18, and 20 for squalenes (Fig. 1) to generate molecules ranging from C_{30} - C_{34} [2]. Additionally, botryococcenes can be found in acyclic or cyclic forms with the ring structures on either end of the molecule,

* Corresponding author.

E-mail address: tpd8@tamuedu (T.P. Devarenne).

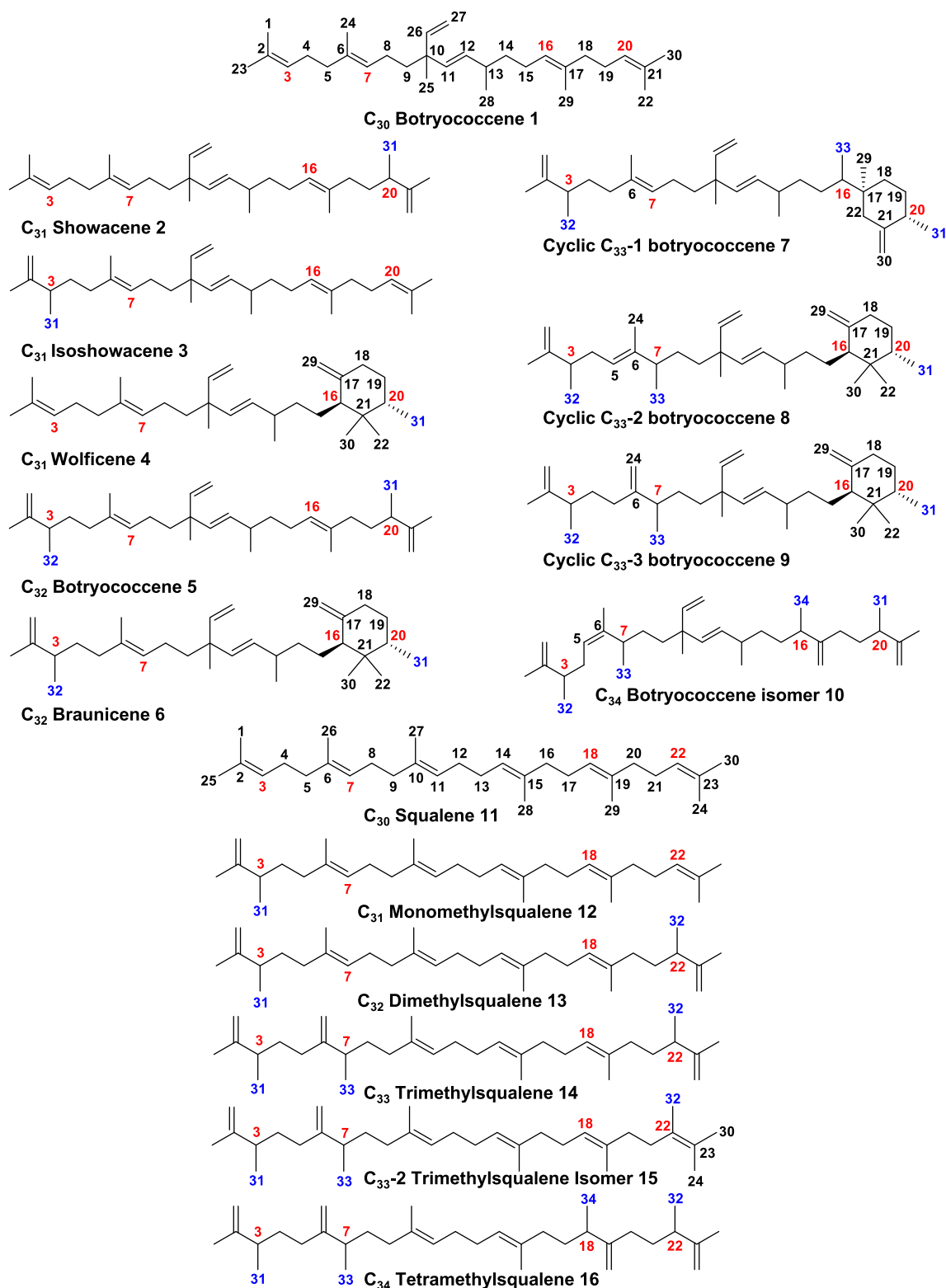


Fig. 1. Hydrocarbons purified from the B race of *B. braunii* for use in Raman spectroscopy for this study.

while methylsqualenes are always acyclic (Fig. 1). This structural diversity has led to the identification of over twenty different botryococcene structures [2,11] and five different methylsqualenes ranging from monomethylsqualene to tetramethylsqualene [12–14] (Fig. 1).

These structural differences between and among botryococenes and methylsqualenes should offer specific spectral signatures that could be used to distinguish between the different molecules. Such information could be useful for monitoring the production of specific hydrocarbons during large scale algal growth

Table 1
Vibrations of *B. braunii* race B botryococenes.

Symbol	Vibration	Showacene 2		Wolficene 4		Braunicene 6		Cyclic C ₃₃ -1 7		Cyclic C ₃₃ -2 8		Cyclic C ₃₃ -3 9		C ₃₄ Botryococcene isomer 10	
		Wavenumber Range (cm ⁻¹)	Number of vibrations	Wavenumber Range (cm ⁻¹)	Number of vibrations	Wavenumber Range (cm ⁻¹)	Number of vibrations	Wavenumber Range (cm ⁻¹)	Number of vibrations	Wavenumber Range (cm ⁻¹)	Number of vibrations	Wavenumber Range (cm ⁻¹)	Number of vibrations	Wavenumber Range (cm ⁻¹)	Number of vibrations
v (CH ₃)	CH ₃ stretch	2886–3045	24	2898–3025	24	2885–3025	24	2886–3044	24	2898–3027	27	2887–3019	24	2871–3045	27
δ (CH ₃)	CH ₃ deformation	1253–1463	24	1345–1474	24	1352–1474	24	1325–1477	24	1322–1474	27	1331–1472	24	1308–1466	27
ρ (CH ₃)	CH ₃ rock	753–1222	16	792–1335	16	555–1329	16	885–1309	16	646–1322	18	477–1306	16	509–1300	18
τ (CH ₃)	CH ₃ torsion	100–285	8	108–319	8	102–335	8	99–290	8	150–316	9	138–315	8	145–302	9
v (CH ₂)	CH ₂ stretch	2872–3117	20	2898–3116	20	2885–3116	22	2886–3116	24	2898–3118	20	2887–3125	24	2871–3119	22
δ (CH ₂)	CH ₂ deformation	1406–1463	10	1411–1474	10	1412–1474	11	1407–1477	12	1366–1474	10	1409–1472	12	1372–1466	11
ω (CH ₂)	CH ₂ wag	916–1377	10	1148–1384	10	907–1363	11	903–1380	12	909–1368	10	909–1366	12	912–1377	11
t (CH ₂)	CH ₂ twist	693–1318	10	729–1332	10	692–1321	11	558–1321	12	691–1335	10	692–1331	12	693–1307	11
ρ (CH ₂)	CH ₂ rock	737–1052	10	729–1033	10	692–1027	11	647–997	12	691–997	10	589–1047	12	536–1013	11
v (CH)	=C–H stretch/ –C–H stretch	2872–3117	8	2898–3044	8	2885–3115	8	2886–3044	8	2898–3027	9	2887–3024	8	2871–3117	9
ω _i (CH)	CH wag (in-plane)	1026–1406	8	1064–1416	8	1078–1378	8	995–1468	8	1061–1439	9	986–1350	8	1022–1408	9
ω _o (CH)	CH wag (out-of-plane)	818–1303	8	813–1345	8	852–1357	8	856–1322	8	857–1370	9	857–1020	8	693–1320	9
v (Ring)	Six-membered ring stretch	–	–	741–1349	6	727–1352	6	736–1414	6	792–1415	6	692–1415	6	–	–
b (Ring)	Six-membered ring bending (in-plane)	–	–	408–486	3	407–692	3	407–647	3	411–646	3	337–594	3	–	–
b (Ring)	Six-membered ring bending (out-of-plane)	–	–	466–693	3	349–709	3	358–707	3	349–691	3	285–647	3	–	–
v (C=C)	C=C stretch	1643–1679	6	1648–1679	5	1650–1670	5	1649–1671	5	1649–1664	5	1649–1663	5	1644–1667	6
v (C–C)	C–C stretch	718–1406	24	713–1411	20	718–1407	21	713–1414	22	712–1415	22	692–1415	22	711–1416	27
b (C–C–C)	C–C–C angle bend	135–632	11	283–693	8	173–709	9	232–707	10	192–691	9	186–714	11	145–629	14
b (C=C–C)	C=C–C angle bend	288–632	10	388–693	5	248–709	6	301–707	6	257–691	6	271–714	6	255–629	7
ω _o (C–CH ₃)	C–CH ₃ wag (out-of-plane)	318–693	8	453–532	8	299–555	8	313–554	8	287–591	9	271–594	8	353–629	9
ω _i (C–CH ₃)	C–CH ₃ wag (in-plane)	272–590	8	297–444	8	231–537	8	266–502	8	234–589	9	246–542	8	239–338	9
τ (C–C)	Internal rotation (C–C)/Skeletal	9–285	16	5–319	18	8–335	19	8–290	20	10–316	19	12–315	20	9–302	18
τ (C=C)	Internal rotation (C=C)/Skeletal	52–285	4	50–319	3	53–335	2	55–290	2	59–316	2	55–315	1	51–302	6
Total		243		243		252		261		261		261		270	

Table 2
Vibrations of *B. braunii* race B squalenes.

Symbol	Vibration	Monomethylsqualene 12		Dimethylsqualene 13		Trimethylsqualene 14		Trimethylsqualene isomer 15		Tetramethylsqualene 16	
		Wavenumber Range (cm ⁻¹)	Number of vibrations	Wavenumber Range (cm ⁻¹)	Number of vibrations	Wavenumber Range (cm ⁻¹)	Number of vibrations	Wavenumber Range (cm ⁻¹)	Number of vibrations	Wavenumber Range (cm ⁻¹)	Number of vibrations
$\nu(\text{CH}_3)$	CH ₃ stretch	2885–3025	24	2887–3025	24	2886–3043	24	2886–3045	27	2886–3024	24
$\delta(\text{CH}_3)$	CH ₃ deformation	1315–1463	24	1315–1462	24	1312–1464	24	1312–1476	27	1341–1463	24
$\rho(\text{CH}_3)$	CH ₃ rock	755–1275	16	735–1221	16	715–1306	16	766–1237	18	575–1307	16
$\tau(\text{CH}_3)$	CH ₃ torsion	72–232	8	74–229	8	87–237	8	70–267	9	87–229	8
$\nu(\text{CH}_2)$	CH ₂ stretch	2885–3116	22	2887–3118	24	2886–3125	26	2886–3125	24	2886–3125	28
$\delta(\text{CH}_2)$	CH ₂ deformation	1372–1463	11	1372–1462	12	1371–1464	13	1372–1476	12	1406–1463	14
$\omega(\text{CH}_2)$	CH ₂ wag	915–1367	11	914–1407	12	914–1377	13	914–1368	12	910–1372	14
$t(\text{CH}_2)$	CH ₂ twist	717–1315	11	716–1304	12	715–1306	13	715–1306	12	713–1307	14
$\rho(\text{CH}_2)$	CH ₂ rock	735–995	11	735–1031	12	734–988	13	736–803	12	736–942	14
$\nu(\text{CH})$	=C–H stretch/C–H stretch	2885–3025	6	2887–3025	6	2886–3009	6	2886–3025	5	2886–3024	6
$\omega_1(\text{CH})$	CH wag (in-plane)	1018–1458	6	1031–1453	6	978–1444	6	1001–1408	5	991–1413	6
$\omega_0(\text{CH})$	CH wag (out-of-plane)	748–1302	6	735–1304	6	573–1306	6	782–1306	5	872–1314	6
$\nu(\text{C}=\text{C})$	C=C stretch	1654–1679	6	1654–1672	6	1652–1672	6	1652–1672	6	1652–1672	6
$\nu(\text{C}-\text{C})$	C–C stretch	717–1408	24	716–1407	25	715–1409	26	707–1412	26	713–1411	27
$b(\text{C}-\text{C}-\text{C})$	C–C–C angle bend	160–596	11	118–598	12	120–595	14	120–597	13	123–595	16
$b(\text{C}=\text{C}-\text{C})$	C=C–C angle bend	232–596	9	260–598	8	237–595	7	292–597	8	277–595	8
$\omega_0(\text{C}-\text{CH}_3)$	C–CH ₃ wag (out-of-plane)	456–583	8	305–580	8	307–586	8	267–597	9	471–579	8
$\omega_1(\text{C}-\text{CH}_3)$	C–CH ₃ wag (in-plane)	330–577	8	260–598	8	237–595	8	247–591	9	238–458	8
$\tau(\text{C}-\text{C})$	Internal rotation (C–C)/Skeletal	6–232	16	5–229	17	7–237	18	6–267	17	6–229	19
$\tau(\text{C}=\text{C})$	Internal rotation (C=C)/Skeletal	53–232	5	54–229	6	52–237	6	53–267	5	42–229	4
Total			243		252		261		261		270

in relation to biofuel feedstock production. Additionally, molecule specific spectral information could be used for mapping cellular/colony locations of each molecule noninvasively by Raman spectroscopy. For example, our past studies analyzing the molecular structure of C₃₀, C₃₂, C₃₃, and C₃₄ botryococenes [15], C₃₀ squalene [16], and the *B. braunii* L race hydrocarbons [17] show that Raman spectroscopy and DFT calculations can be used to identify spectral differences in the $\nu(\text{C}=\text{C})$ stretch for these molecules to differentiate between them. In the current study, we report the assignment of bond frequencies for seven botryococenes not before reported and five methylsqualenes based on experimental and DFT calculations. Additionally, ten botryococenes are analyzed using various Raman spectroscopy techniques to show this approach can be used to distinguish between several of these molecules.

2. Experimental methods

2.1. Culturing of *B. braunii*

B. braunii race B, Showa (Berkeley) strain [18], was grown at 22 °C under continuous aeration with filter-sterilized air enriched with 2.5% CO₂. A modified Chu 13 media was used for culturing [19]. Cultures were exposed to a light intensity of 120 $\mu\text{mole photons} \cdot \text{m}^{-2} \cdot \text{s}^{-1}$ under a 12:12 h light:dark cycle. Algal cultures were subcultured from a six-week-old culture using 100 ml of floating colonies for inoculation into 750 ml of fresh medium.

2.2. Hydrocarbon purification

B. braunii B race hydrocarbons were purified as previously described [14,20,21]. Briefly, five-week-old freeze-dried algal colonies were treated three times with *n*-hexane to extract extracellular hydrocarbons, followed by two treatments with CHCl₃:MeOH (2:1) to extract intracellular hydrocarbons. Solvents from both extracts were removed using a rotary evaporator, the hydrocarbons resuspended in a minimal amount of *n*-hexane, the extracts combined, and applied to a gravity-fed silica gel column using *n*-hexane as the mobile phase. The eluent collected prior to the pigment front was pooled as the total hydrocarbon fraction, the solvent removed using a rotary evaporator, the hydrocarbons resuspended in a small amount of *n*-hexane, and a crude separation of the hydrocarbons into eight peaks was done by reversed-phase HPLC using a Cosmosil 5C₁₈-AR-II column (20 mm × 250 mm) with 100% MeOH as the mobile phase at a flow rate of 8 ml/min and detection at 210 nm. Each peak from this separation contained multiple molecules, which were further separated using normal-phase HPLC using a Develosil 60 silica column (20 mm × 250 mm) with 100% *n*-hexane as the mobile phase at a flow rate of 8 ml/min and detection at 210 nm. Peaks that still contained multiple molecules were further separated by normal-phase HPLC using a KANTO silver nitrate (AgNO₃) silica column (4.6 × 250 mm) with 99.85%:0.15% *n*-hexane:acetonitrile as the mobile phase at a flow rate of 1 ml/min and detection at 210 nm. Purity to at least 95% and molecular mass of each sample was determined by GC–MS analysis, and molecule structure identity confirmed by NMR analysis [14].

2.3. Raman spectroscopy

Experimental Raman spectroscopy data was collected using line-scan and broadband coherent anti-Stokes Raman spectroscopy (BCARS). For all spectroscopy, each hydrocarbon was dissolved in *n*-hexane and ~100 μg of each sample was pipetted onto a glass microscope slide one drop at a time, allowing the *n*-

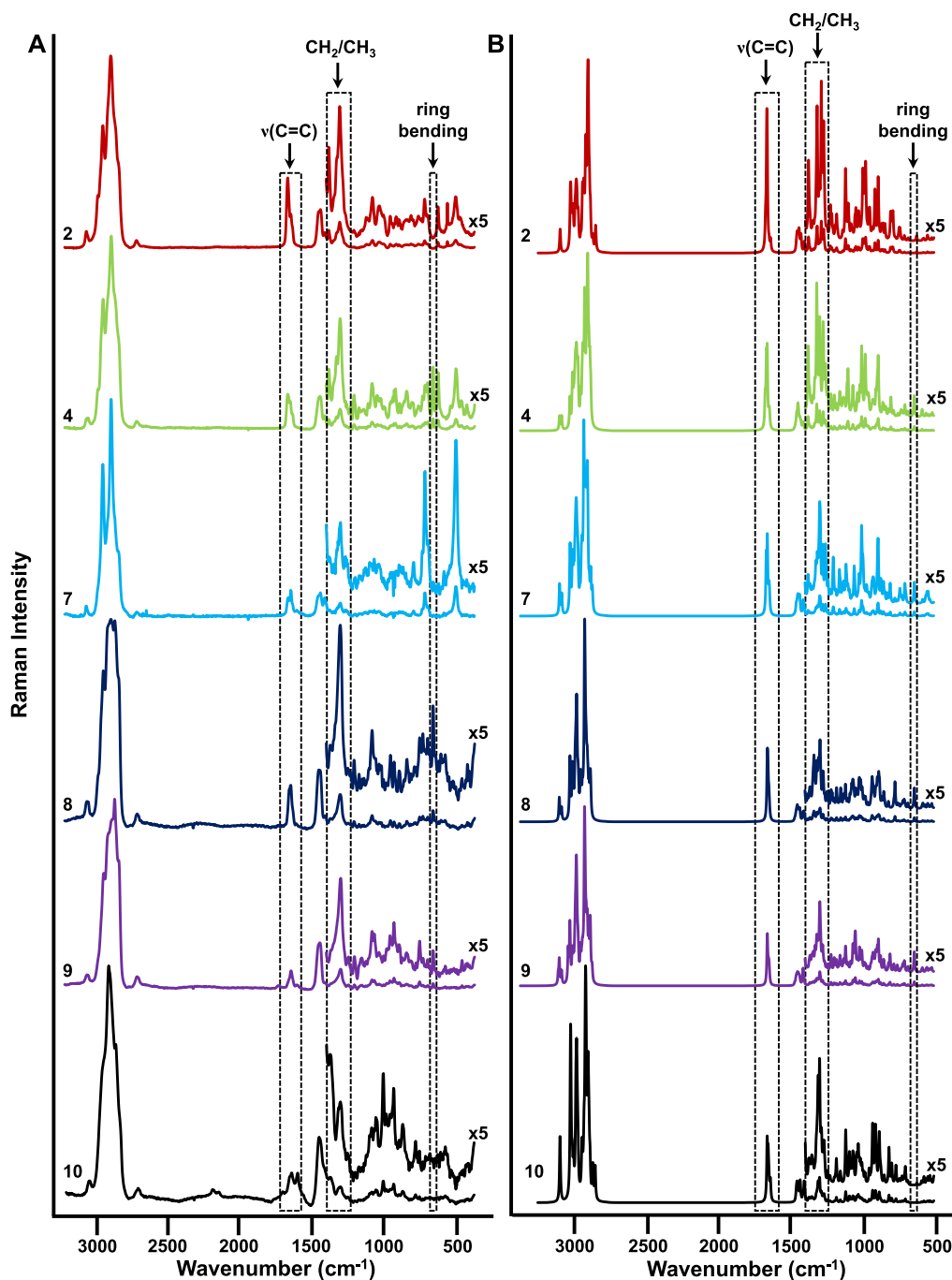


Fig. 2. Experimental and calculated spectra for botryococenes. **A.** The experimental Raman spectra for the indicated botryococenes. **B.** The calculated Raman spectra for the indicated botryococenes. Spectral regions in dashed line boxes indicate the $\nu(\text{C}=\text{C})$ stretching analyzed in Fig. 4A and B, CH_2/CH_3 bending analyzed in Fig. 5A and B, and cyclohexane b(Ring) bending analyzed in Fig. 6A and B.

hexane to evaporate after applying each drop. Once all *n*-hexane was evaporated the spectra for each hydrocarbon was collected.

Line-scan Raman spectroscopy analysis was carried out on the following purified hydrocarbons: C_{31} showacene **2**, C_{31} wolficene **4**, cyclic C_{33} -1 botryococcene **7**, cyclic C_{33} -2 botryococcene **8**, and cyclic C_{33} -3 botryococcene **9**, C_{34} botryococcene isomer **10**, monomethylsqualene **12**, dimethylsqualene **13**, trimethylsqualene **14**, trimethylsqualene isomer **15**, and tetramethylsqualene **16**. For data acquisition, line-scan Raman was carried out as previously reported [22]. Briefly, the output of a continuous-wave 532 nm laser (Spectra-Physics Millennia Xs) was focused on the sample as a

uniform $133 \times 1 \mu\text{m}^2$ line. Epi-Raman was collected by a $60\times$ objective (Olympus, N.A = 1.2), imaged at the entrance slit of a spectrograph (Acton 2300) and recorded by a CCD detector (PIXIS 400BR). All spectra were collected at 35 mW of power using 4 min exposure. A fifth order polynomial least-squares fitting algorithm was used for spectral baseline correction.

BCARS analysis was carried out on the following purified hydrocarbons: C_{30} botryococcene **1**, C_{31} isoshowacene **3**, C_{32} botryococcene **5**, and C_{32} braunicene **6**. Each hydrocarbon was separately dried on a glass microscope slide within a gasket, then covered with a coverslip. BCARS-generated Raman spectra were collected on a

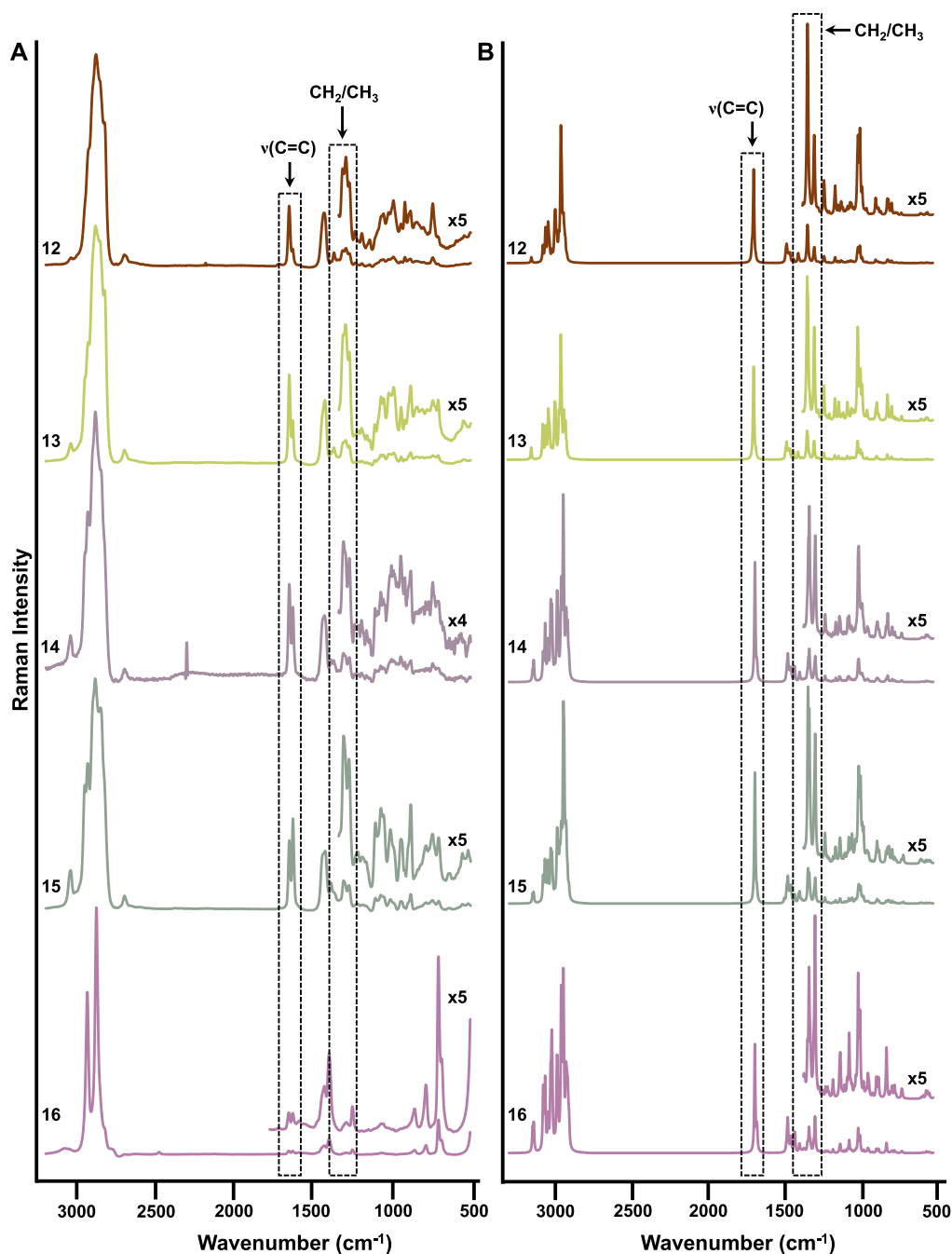


Fig. 3. Experimental and calculated spectra for methylsqualenes. **A.** The experimental Raman spectra for the indicated methylsqualenes. **B.** The calculated Raman spectra for the indicated methylsqualenes. Spectral regions in dashed line boxes indicate the $\nu(\text{C}=\text{C})$ stretching analyzed in Fig. 4C and D, and CH_2/CH_3 bending analyzed in Fig. 5C and D.

100×100 pixel grid with $2 \mu\text{m}/\text{pixel}$ spacing. Described previously [23], the BCARS instrument employs a 40 MHz dual-output fiber laser, with a 16 mW, 770 nm probe output of pulse duration 3.4 ps, and a 10 mW, 900 nm-centered supercontinuum output with 16 fs duration. This system provides Raman spectra at each image pixel with a pixel dwell time of 3.5 ms.

2.4. Theoretical computations

The vibrational frequencies and Raman intensities of all twelve molecules were calculated using the Gaussian 09 program, Revision A.02 [24]. The density functional theory (DFT) B3LYP method

[25,26] was utilized with a cc-pVTZ basis set for the computations. The calculations apply for the vapor-phase of these molecules, but little difference between these values and those for the liquid state is expected except for the low frequency modes below about 200 cm^{-1} . The standard Gaussian 09 protocol with the default values for bandwidths was used for producing the computed spectra in the figures. The Semichem AMPAC/AGUI program [27] was utilized to visualize the vibrational modes. A scaling factor of 0.969 was used for all frequencies above 1000 cm^{-1} and 0.985 was used for the lower frequencies. These scaling factors values were found to be best suited for correlating the experimental and theoretical frequency values in our previous studies [15–17,28].

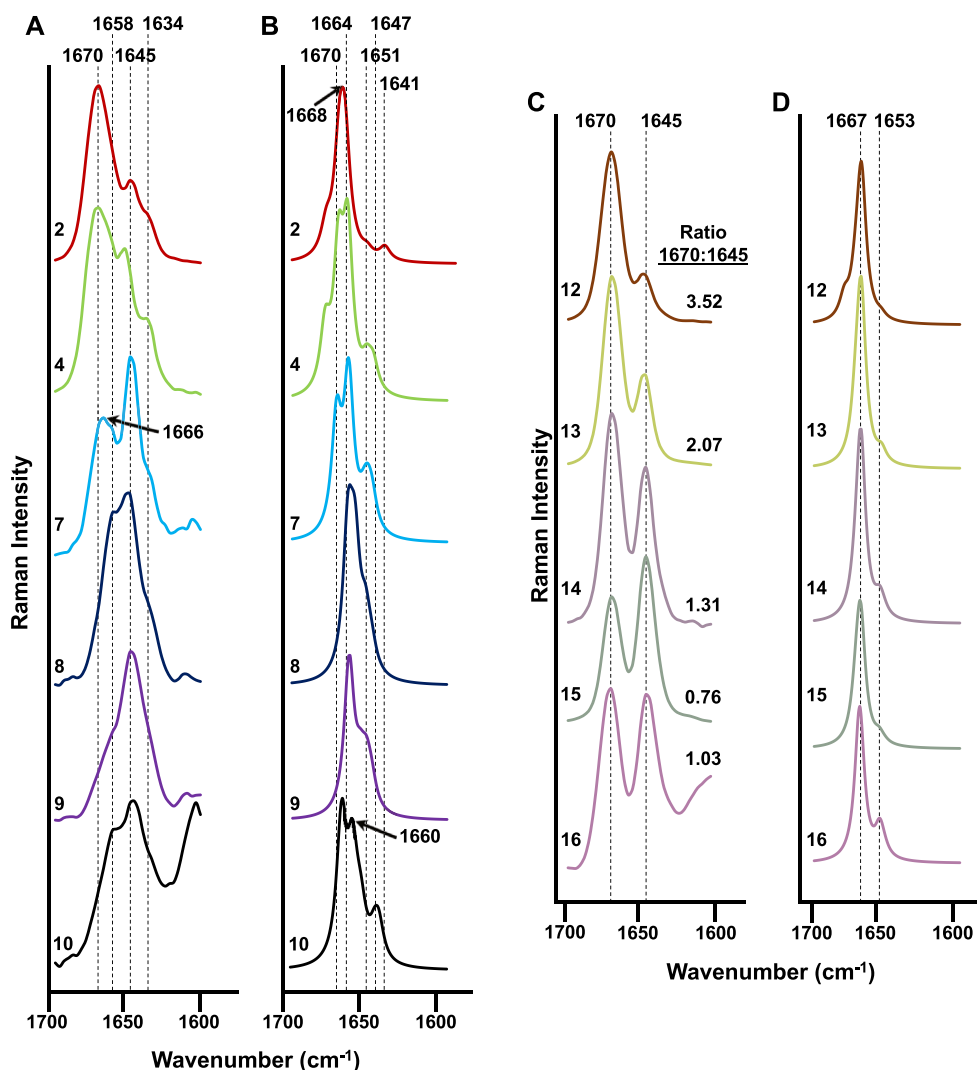


Fig. 4. The experimental and calculated $\nu(\text{C}=\text{C})$ stretching Raman spectral regions for botryococenes and methylsqualenes. **A.** Experimental spectral region for the indicated botryococenes. **B.** Calculated spectral region for the indicated botryococenes. **C.** Experimental spectral region for the indicated methylsqualenes. **D.** Calculated spectral region for methylsqualenes.

Those previous studies also showed that on the whole the vibrational frequencies changed insignificantly for the different conformational orientations of these types of molecules.

3. Results and discussion

3.1. Density function theory (DFT) computations for bond frequencies of *B* race hydrocarbons

The number of atoms (N) in these molecules ranges from 83 to 92, and thus the molecules possess 243 to 270 ($3N-6$) vibrational modes of varying Raman intensity resulting in very complex spectra. The individual vibrational assignments are too lengthy to detail, but **Tables 1 and 2** present a summary of the types of vibrations for each molecule. The C–H and C=C stretching vibrations are distinct but all of the other vibrational motions are strongly coupled. The computed spectra themselves are presented in **Figs. 2–6** and will be discussed below in comparison to the experimental spectra. The focus of this study is the application of Raman spectroscopy to the identification of these molecules and to distinguish between them. The most useful spectral region for this

study is the $\nu(\text{C}=\text{C})$ stretch region in the 1600 to 1700 cm^{-1} range for these molecules. Other Raman bands in the lower frequency “finger print region” are also characteristic of several of these molecules and these will be discussed below.

3.2. Comparison of experimental and calculated full Raman spectra for *B* race hydrocarbons

Based on our past Raman spectroscopy studies on *B. braunii* hydrocarbons from the B and L races [15,17] as well as non-methylated C_{30} squalene [16], we have found several spectral regions that can be used to distinguish between these structurally similar molecules. Specifically, these regions are the $\nu(\text{C}=\text{C})$ stretching region between 1600 and 1700 cm^{-1} , and the CH_2/CH_3 bending, $\omega_i(\text{CH})$ wag (in-plane), and $\nu(\text{C}-\text{C})$ stretching region between 1250 and 1400 cm^{-1} (this region will be referred to as CH_2/CH_3 bending for simplicity). Additionally, based on the DFT calculations shown in **Table 1** the cyclohexane b(Ring) bending (in-plane and out-of-plane) region between 630 and 665 cm^{-1} should provide a specific spectral signature to clearly distinguish the cyclic botryococenes from the acyclic botryococenes. These spectral

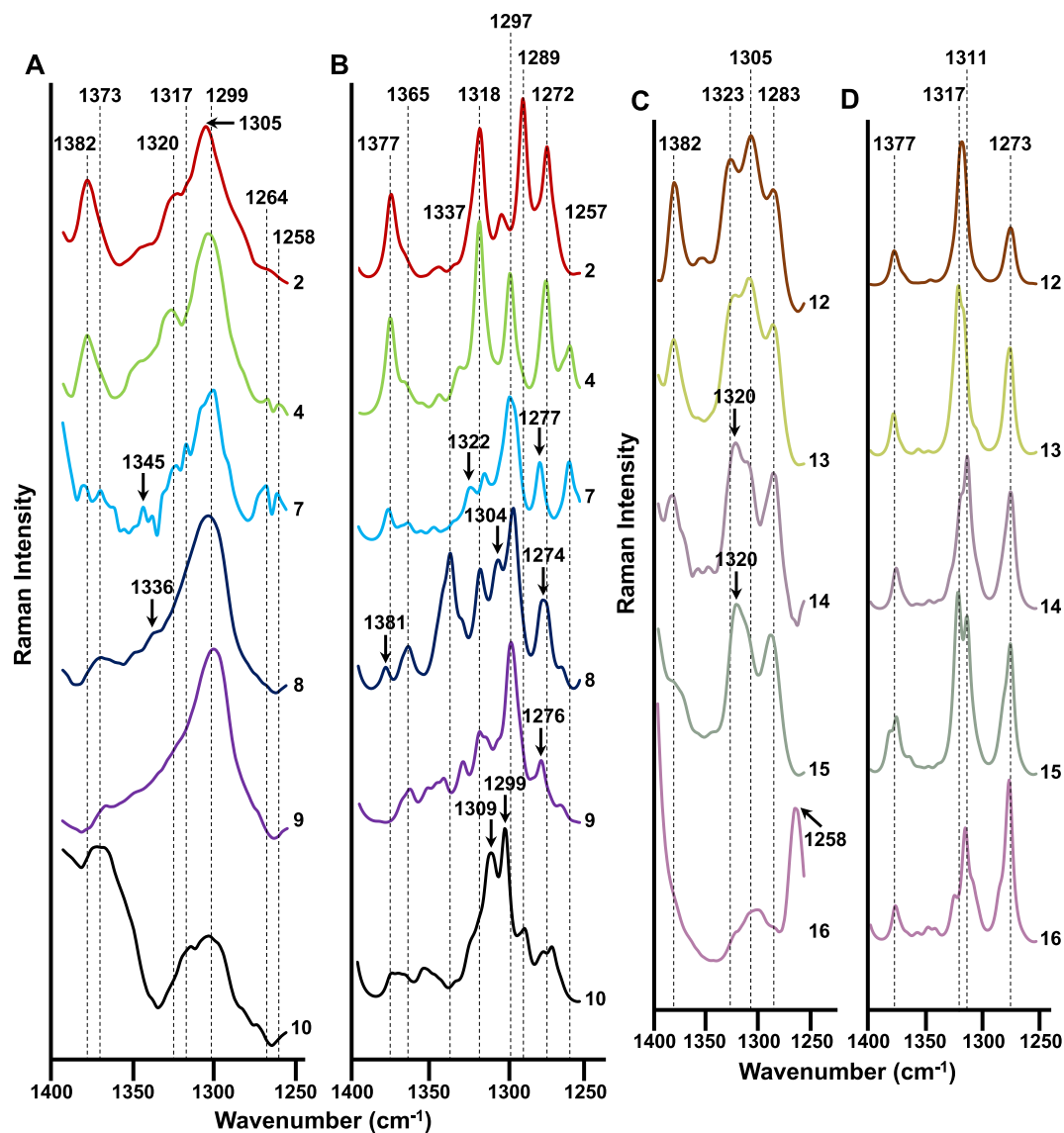


Fig. 5. The experimental and calculated Raman spectral regions containing $\delta(\text{CH}_2)$ deformation, $\rho(\text{CH}_2)$ rock, $\omega(\text{CH}_2)$ wag, $\tau(\text{CH}_2)$ twist, $\omega_i(\text{CH})$ wag (in-plane), and $\nu(\text{C}=\text{C})$ stretch for botryococcenes and methylsqualenes. **A.** Experimental spectral region for the indicated botryococcenes. **B.** Calculated spectral region for the indicated botryococcenes. **C.** Experimental spectra region for the indicated methylsqualenes. **D.** Calculated spectral region for the indicated methylsqualenes.

regions were analyzed experimentally by subjecting two acyclic botryococcenes, C_{31} botryococcene **2** and C_{34} botryococcene isomer **10**, and 4 cyclic botryococcenes, C_{31} wolficene **4**, C_{33-1} cyclic botryococcene **7**, C_{33-2} cyclic botryococcene **8**, and C_{33-3} cyclic botryococcene **9**, to line-scan Raman spectroscopy. Additionally, the computed spectra were compared to the experimental spectra. None of these botryococcenes have been studied by Raman spectroscopy previously.

Comparing the experimental (Fig. 2A) and computed (Fig. 2B) spectra for each botryococcene shows a strong correlation between the two types of spectra, with high similarity in the $\nu(\text{C}=\text{C})$ stretching and CH_2/CH_3 bending regions for all molecules. Comparing the spectra between acyclic and cyclic botryococcenes, the cyclohexane b(Ring) bending region shows an obvious Raman band in the cyclic botryococcenes in the $630\text{--}665\text{ cm}^{-1}$ region that is lacking from the acyclic botryococcenes (Fig. 2A and B). In addition, there are some differences between each molecule in the $\nu(\text{C}=\text{C})$ stretching and CH_2/CH_3 bending regions. For example, the intensity of the Raman bands varies between molecules in both of

these regions, and some molecules have a single band while others have two bands in these regions (Fig. 2A and B). These differences will be discussed in detail below.

The same comparative analysis was carried out for the methylsqualenes. As with the botryococcenes, the experimental (Fig. 3A) and computational (Fig. 3B) spectra show a strong correlation for each methylsqualene. A comparison of the spectra between methylsqualenes indicates that in the CH_2/CH_3 bending region there is a high degree of similarity with two or three Raman bands for each molecule (Fig. 3A and B). However, while each methylsqualene has a Raman band doublet in the $\nu(\text{C}=\text{C})$ stretching region, the intensity of each band differs for each molecule (Fig. 3A). The ratio between these two bands should be a diagnostic signal for each molecule. These differences will be discussed in detail below.

3.3. Raman spectral regions that can distinguish between hydrocarbons

A detailed analysis of the $\nu(\text{C}=\text{C})$ stretching, CH_2/CH_3 bending,

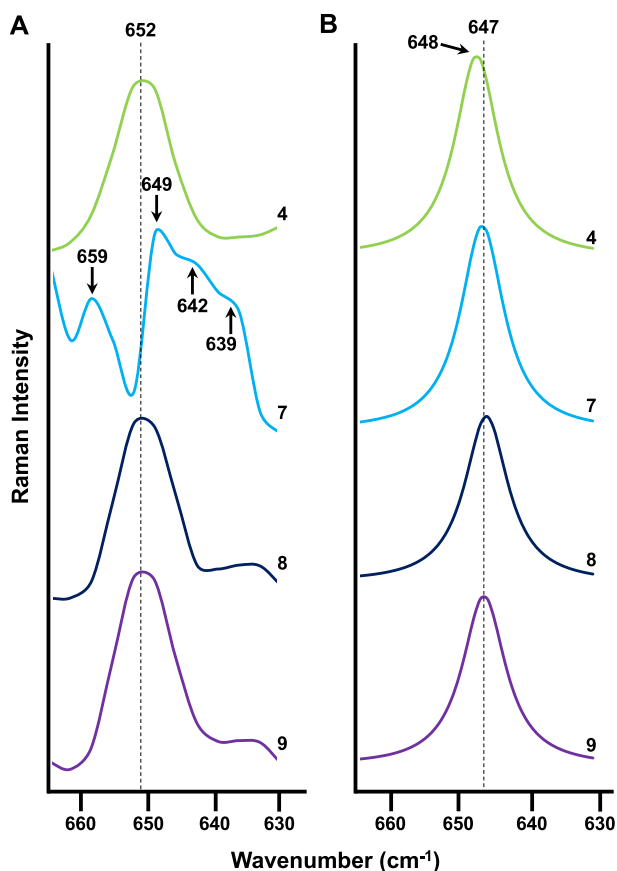


Fig. 6. The experimental and calculated cyclohexane b(Ring) bending Raman spectral regions for botryococcenes. **A.** Experimental spectral region for the indicated botryococcenes. **B.** Calculated spectral region for the indicated botryococcenes.

and cyclohexane b(Ring) bending regions for all hydrocarbons analyzed indicates these regions can be used to distinguish between several of these molecules. For the $\nu(\text{C}=\text{C})$ stretching region ($1600\text{--}1700\text{ cm}^{-1}$) of the botryococcenes analyzed there is a clear distinction between the predominant Raman band for **2** and **4** compared to **7**, **8**, and **9**. For **2** and **4**, there is a strong Raman band in the 1670 cm^{-1} region (Fig. 4A). In **7** there is a Raman band of moderate intensity in the 1670 cm^{-1} region (at 1666 cm^{-1}), but the most prominent band is at 1645 cm^{-1} . The spectra for **8**, **9**, **10** show no Raman band in the 1670 cm^{-1} region, rather the strongest Raman band is shifted to 1645 cm^{-1} (Fig. 4A). Additionally, bands at 1634 cm^{-1} in **2**, **4**, **7** and 1658 cm^{-1} in **8**, **9**, **10** can also be used to distinguish between these molecules (Fig. 4A). These experimental observations are well supported by the Raman bands seen in the calculated spectra (Fig. 4B).

The $\nu(\text{C}=\text{C})$ stretching region for the experimental analysis of methylsqualenes shows two Raman bands for each molecule at 1670 cm^{-1} and 1645 cm^{-1} (Fig. 4C). It can be seen that as the methylation status of the squalenes increases from monomethylation in **12** to tetramethylation in **16** the intensity of the 1670 cm^{-1} band remains roughly the same while the 1645 cm^{-1} band increases (Fig. 4C). The difference between these molecules is the position of the $\text{C}=\text{C}$ bonds. As the squalenes are methylated the backbone $\text{C}=\text{C}$ bonds at positions 2, 6, 18, and 22 migrate to exomethylene groups at carbon positions 1, 26, 29, and 24 (Fig. 1). Thus, as the squalenes are methylated the number of backbone $\text{C}=\text{C}$ bonds decreases and the number of exomethylene $\text{C}=\text{C}$ bonds increases. From this information the 1670 cm^{-1} Raman band can be

assigned to the backbone $\text{C}=\text{C}$ bonds and the 1645 cm^{-1} band can be assigned to the exomethylene $\text{C}=\text{C}$ bonds. The calculated $1670:1645$ ratio for the intensities between these two bands shows there is a clear distinction in this value for each methylsqualene that could be used to distinguish between each molecule (Fig. 4C). Interestingly, these experimental observations are not well supported by the calculated spectra for the methylsqualenes, which shows a single predominant Raman band at 1667 cm^{-1} for each methylsqualene (Fig. 4D).

As with our previous studies [15–17], for all molecules analyzed the DFT calculations predict a number of $\nu(\text{C}=\text{C})$ stretching frequencies equal to the number of $\text{C}=\text{C}$ bonds in each molecule (Tables 1 and 2). However, the experimental spectra do not show all of these $\nu(\text{C}=\text{C})$ stretching Raman bands (Fig. 4A, C). This is due to the fact that several $\text{C}=\text{C}$ stretching bands are very close in frequency, thus generating a few predominant bands caused by spectral overlap.

For the CH_2/CH_3 bending region ($1250\text{--}1400\text{ cm}^{-1}$), the experimental spectra have many similarities for the botryococcenes analyzed with a main, broad Raman band centered around 1299 cm^{-1} (Fig. 5A). However, a band at 1382 cm^{-1} can be used to distinguish **2**, **4**, and **7** from the other botryococcenes (Fig. 5A). As was seen for the $\nu(\text{C}=\text{C})$ stretching frequencies, the calculated spectra (Fig. 5B) and the calculated vibrations (Table 1) predict many CH_2/CH_3 vibrations in the $1250\text{--}1400\text{ cm}^{-1}$ region that are not clearly defined in the experimental spectra. Again, this is likely due to spectral overlap of vibrations within very close frequencies. Similarly, the CH_2/CH_3 bending region of the experimental spectra for the methylsqualenes shows a high degree of similarity for each molecule with several predominant Raman bands between 1283 cm^{-1} and 1323 cm^{-1} (Fig. 5C). A band at 1282 cm^{-1} can distinguish **12**, **13**, and **14** from the other methylsqualenes while **16** has a band at 1258 cm^{-1} not seen in the other molecules (Fig. 5C). The calculated spectra confirm the main Raman bands in the $1273\text{--}1323\text{ cm}^{-1}$ region (Fig. 5D).

The ring structures found in botryococcenes **4**, **7**, **8**, and **9**, should offer unique vibrations that can distinguish these molecules from the acyclic botryococcenes. In the experimental spectra, the $630\text{--}665\text{ cm}^{-1}$ region for the cyclohexane b(Ring) bending vibrations shows a Raman band at 652 cm^{-1} that is found in **4**, **8**, and **9**, while the main band for **7** is broad with a peak at 649 cm^{-1} and shoulders at 642 cm^{-1} and 639 cm^{-1} (Fig. 6A). An additional band at 659 cm^{-1} can also distinguish **7** from the other cyclic botryococcenes (Fig. 6A). These bands are not seen for the acyclic botryococcenes **2** and **10** (Fig. 2). Molecules **4**, **8**, and **9** all have the same ring structure with cyclization at carbon 16 (Fig. 1), and thus it is not surprising that the spectra for these molecules within this region are nearly identical (Fig. 6A). For molecule **7**, the ring is cyclized at carbon 17 (Fig. 1) generating the spectral differences seen. It should be noted that the intensity of the bands shown for **7** in Fig. 6A have been scaled in order to have the bands stand out. However, in absolute values the intensity of these bands for **7** are much lower than that observed for **4**, **8**, and **9** within this ring bending region (Fig. 2). The calculated spectra for the cyclic botryococcenes largely agree with the experimental spectra except for molecule **7**, which shows a single Raman band at 647 cm^{-1} (Fig. 6B).

3.4. Distinguishing between botryococcene isomers using broadband CARS

We next attempted to distinguish between several botryococcenes using broadband coherent anti-Stokes Raman spectroscopy (BCARS). The botryococcenes used, C_{30} botryococcene **1**, C_{31} isoshowacene **3**, C_{32} botryococcene **5**, and C_{32} braunicene **6**, were

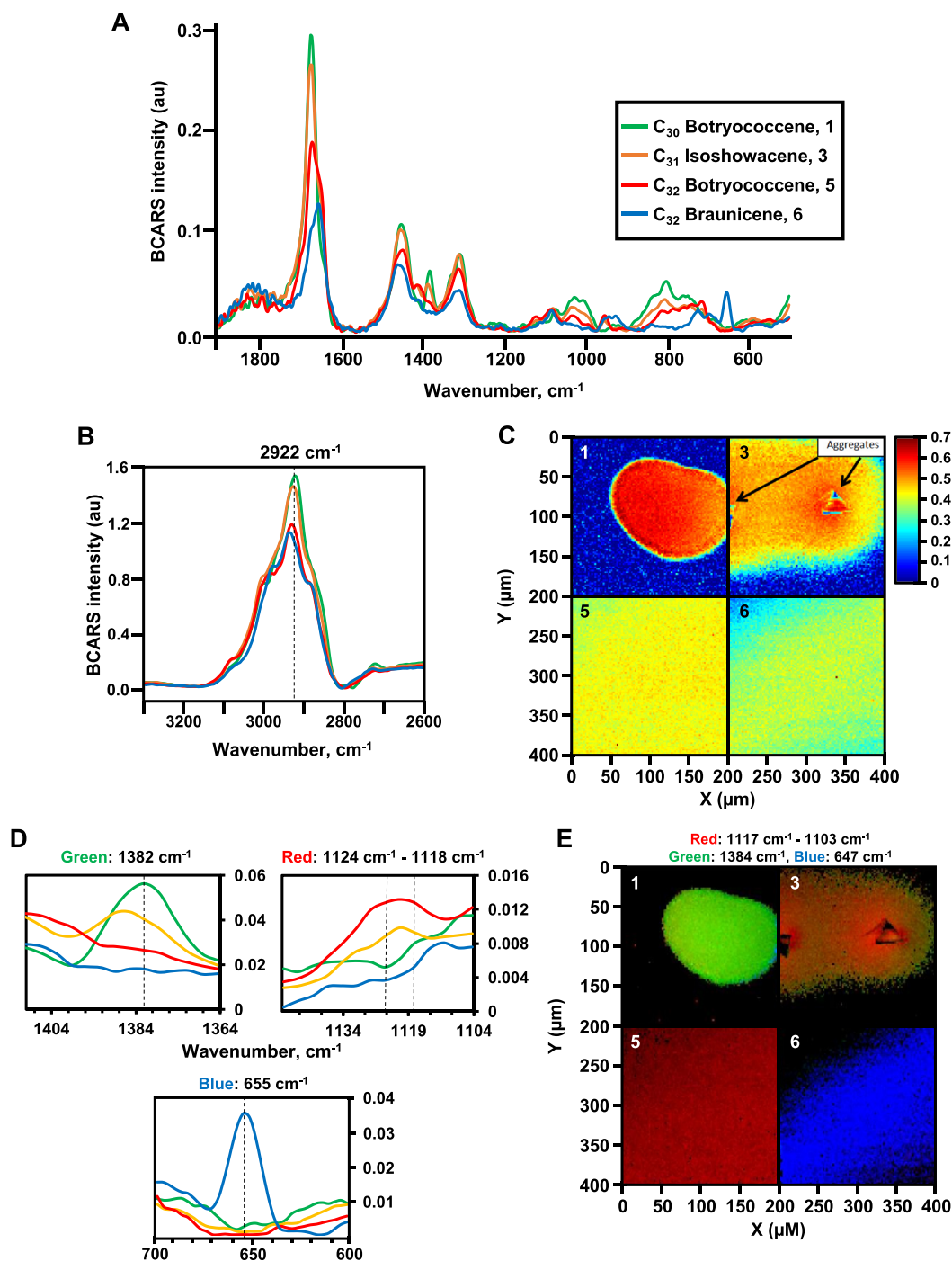


Fig. 7. Spectral differentiation of C_{30} botryococcene 1, C_{31} isoshowacene 3, C_{32} botryococcene 5, and C_{32} braunicene 6 by BCARS. **A.** The experimental BCARS spectra for the indicated botryococcenes. The colored line indicated for each botryococcene applies to all spectra shown throughout the figure. **B.** The BCARS C–H stretching spectral region for the indicated botryococcenes. Dotted vertical line marks wavenumber 2935 cm^{-1} analyzed in C. **C.** Detection of the indicated botryococcenes based on detection of the 2935 cm^{-1} wavenumber. Scale of intensity detection is shown on the right side of this panel. **D.** Specific BCARS spectral signatures for the indicated botryococcenes used for analysis in E. Vertical dotted lines indicate specific wavenumber or wavenumber region analyzed. **E.** Each botryococcene spotted on a glass slide was scanned for each BCARS spectral signature shown in D, indicating that each molecule can be distinguished from each other by this method.

chosen because analysis of these molecules should indicate if Raman spectroscopy can distinguish between the structurally similar acyclic isomers and one cyclic isomer. The BCARS spectra for these molecules in the fingerprint region ($500\text{--}1900\text{ cm}^{-1}$) indicate a high degree of similarity between the molecules (Fig. 7A). However, several regions will be highlighted that can be used to distinguish each of these molecules.

First, each molecule was analyzed to confirm detection using the BCARS system by analyzing the intensity of the general C–H stretch for each molecule. Each botryococcene was spotted on a glass slide, analyzed by BCARS, and the intensity of the C–H stretching signal at 2922 cm^{-1} (Fig. 7B) mapped onto each molecule on the glass slide (Fig. 7C). The intensity of the 2922 cm^{-1} C–H stretching signal can be easily detected for each molecule indicating BCARS can be

used for analysis of these molecules. Additionally, it can be seen that each molecule has different surface tension characteristics. The C₃₀ botryococcene **1** stayed as a tight oil drop on the glass slide while each of the other botryococcenes spread out more on the surface of the glass slide and were no longer contained in a tight oil drop such as for C₃₂ braunicene **6** (Fig. 7C).

Next, three spectral regions that should offer specificity to several of these botryococcenes were analyzed. These three regions were identified from the fingerprint region of each spectrum and then each botryococcene was analyzed for the detection of each signal. The first region analyzed was a Raman band at 1382 cm⁻¹ that is mainly found in the spectrum for C₃₀ botryococcene **1** (Fig. 7D). Each botryococcene was analyzed for a signal from the 1382 cm⁻¹ band, and if it was detected the signal was assigned a green color for mapping to the hydrocarbons on the glass slide. It can be seen that the 1382 cm⁻¹ signal was mainly found in C₃₀ botryococcene **1** with lower detection in C₃₁ isoshowacene **3**, and no detection in either C₃₂ botryococcene **5** or C₃₂ braunicene **6** (Fig. 7E). The second spectral region analyzed was a Raman band between 1124 cm⁻¹ and 1118 cm⁻¹ that is mostly detected in C₃₂ botryococcene **5** (Fig. 7D). If the signal for the 1124–1118 cm⁻¹ region was detected in any molecule it was given a red color for mapping to the hydrocarbons on the glass slide. This signal was mainly detected in C₃₂ botryococcene **5** with lower detection in C₃₁ isoshowacene **3**, and no detection in C₃₀ botryococcene **1** or C₃₂ braunicene **6** (Fig. 7E). Interestingly, C₃₂ botryococcene **5** is mainly shown as an orange color which would be due to mixed detection of the green 1382 cm⁻¹ signal and the red 1124–1118 cm⁻¹ signal (Fig. 7E). The third spectral region analyzed was a Raman band at 655 cm⁻¹ that is specific for the cyclohexane b(Ring) bending in C₃₂ braunicene **6** (Fig. 7D). Detection of the 655 cm⁻¹ signal in any molecule was assigned a blue color, and this signal is only detected in C₃₂ braunicene **6** (Fig. 7E).

4. Conclusions

Distinguishing between structurally similar molecules by spectroscopy techniques such as the *B. braunii* race B hydrocarbons is challenging. Here we have shown that experimental and calculated Raman spectroscopy can be used to clearly differentiate between several of these hydrocarbons. This information could be used for commercial production of algal hydrocarbons. For example, particular hydrocarbons may be more suited for certain industrial applications, and thus more desirable. The use of Raman spectroscopy to identify production levels of these particular hydrocarbons within an algal culture would then inform best times for harvest to maximize hydrocarbon production.

Acknowledgments

This work was supported by the National Science Foundation [grant number EFRI-PSBR #1240478 TPD] and the Robert A. Welch Foundation [grant A-0396 to J.L.]. Computations were carried out on the Texas A&M Department of Chemistry Medusa computer system funded by the National Science Foundation [grant CHE-0541587].

References

- [1] Q. Hu, M. Sommerfeld, E. Jarvis, M. Ghirardi, M. Posewitz, M. Seibert, A. Darzins, Microalgal triacylglycerols as feedstocks for biofuel production: perspectives and advances, *Plant J.* 54 (2008) 621–639.
- [2] P. Metzger, C. Largeau, *Botryococcus braunii*: a rich source for hydrocarbons and related ether lipids, *Appl. Microbiol. Biotechnol.* 66 (2005) 486–496.
- [3] J.M. Moldowan, W.K. Seifert, First discovery of botryococcane in petroleum, *J.C.S. Chem. Comm* 19 (1980) 912–914.
- [4] D.M. McKirdy, R.E. Cox, J.K. Volkman, V.J. Howell, Botryococcanes in a new class of Australian non-marine crude oils, *Nature* 320 (1986) 57–59.
- [5] E. Lichtfouse, S. Derenne, A. Mariotti, C. Largeau, Possible algal origin of long-chain odd *n*-alkanes in immature sediments as revealed by distributions and carbon-isotope ratios, *Org. Geochem* 22 (1994) 1023–1027.
- [6] M. Glikson, K. Lindsay, J. Saxby, *Botryococcus* - a planktonic green alga, the source of petroleum through the ages: transmission electron microscopical studies of oil shales and petroleum source rocks, *Org. Geochem* 14 (1989) 595–608.
- [7] P. Adam, P. Schaeffer, P. Albrecht, C₄₀ monoaromatic lycopane derivatives as indicators of the contribution of the alga *Botryococcus braunii* race L to the organic matter of Messel oil shale (Eocene, Germany), *Org. Geochem* 37 (2006) 584–596.
- [8] L.W. Hillen, G. Pollard, L.V. Wake, N. White, Hydrocracking of the oils of *Botryococcus braunii* to transport fuels, *Biotechnol. Bioeng.* 24 (1982) 193–205.
- [9] H. Kitazato, S. Asaoka, H. Iwamoto, Catalytic cracking of hydrocarbons from microalgae, *Sekiyu Gakkaishi* 32 (1989) 28–34.
- [10] N.H. Tran, J.R. Bartlett, G.S.K. Kannangara, A.S. Milev, H. Volk, M.A. Wilson, Catalytic upgrading of biorefinery oil from micro-algae, *Fuel* 89 (2010) 265–274.
- [11] A. Banerjee, R. Sharma, Y. Chisti, U.C. Banerjee, *Botryococcus braunii*: a renewable source of hydrocarbons and other chemicals, *Crit. Rev. Biotechnol.* 22 (2002) 245–279.
- [12] E. Achitouv, P. Metzger, M.N. Rager, C. Largeau, C₃₁–C₃₄ methylated squalenes from a Bolivian strain of *Botryococcus braunii*, *Phytochem* 65 (2004) 3159–3165.
- [13] Z. Huang, C.D. Poulter, Tetramethylsqualene, a triterpene from *Botryococcus braunii* var. *showa*, *Phytochem* 28 (1989) 1467–1470.
- [14] M. Tatli, M.T. Naik, S. Okada, L.J. Dangott, T.P. Devarenne, Isolation and characterization of cyclic C₃₃ botryococcenes and a trimethylsqualene isomer from *Botryococcus braunii* Race B, *J. Nat. Prod.* 80 (2017) 953–958.
- [15] T.L. Weiss, H.J. Chun, S. Okada, S. Vitha, A. Holzenburg, J. Laane, T.P. Devarenne, Raman spectroscopy analysis of botryococcene hydrocarbons from the green microalga *Botryococcus braunii*, *J. Biol. Chem.* 285 (2010) 32458–32466.
- [16] H.J. Chun, T.L. Weiss, T.P. Devarenne, J. Laane, Vibrational spectra and DFT calculations of squalene, *J. Mol. Struct.* 1032 (2013) 203–206.
- [17] H.J. Chun, S. Waqued, H.R. Thapa, A. Han, V.V. Yakovlev, J. Laane, T.P. Devarenne, Raman spectra and DFT calculations for tetraterpene hydrocarbons from the L race of the green microalga *Botryococcus braunii*, *J. Mol. Struct.* 1129 (2017) 216–221.
- [18] A.M. Nonomura, *Botryococcus braunii* var. *showa* (Chlorophyceae) from Berkeley, California, United States of America, *Jpn. J. Phycol.* 36 (1988) 285–291.
- [19] S.P. Chu, The influence of the mineral composition of the medium on the growth of planktonic algae Part 1. Methods and culture media, *J. Ecol.* 30 (1942) 284–325.
- [20] S. Okada, M. Murakami, K. Yamaguchi, Hydrocarbon composition of newly isolated strains of the green microalga *Botryococcus braunii*, *J. Appl. Phycol.* 7 (1995) 555–559.
- [21] S. Okada, M. Murakami, K. Yamaguchi, Characterization of hydrocarbons from the Yayoi strain of the green microalga *Botryococcus braunii*, *Phytochem. Anal.* 8 (1997) 198–203.
- [22] J. Qi, W.C. Shih, Performance of line-scan Raman microscopy for high-throughput chemical imaging of cell population, *Appl. Opt.* 53 (2014) 2881–2885.
- [23] C.H. Camp Jr., Y.J. Lee, J.M. Heddleston, C.M. Hartshorn, A.R. Hight Walker, J.N. Rich, J.D. Lathia, M.T. Cicerone, High-speed coherent raman fingerprint imaging of biological tissues, *Nat. Photonics* 8 (2014) 627–634.
- [24] M.J. Frisch, G.W. Trucks, H.B. Schlegel, G.E. Scuseria, M.A. Robb, J.R. Cheeseman, G. Scalmani, V. Barone, B. Mennucci, G.A. Petersson, H. Nakatsuji, M. Caricato, X. Li, H.P. Hratchian, A.F. Izmaylov, J. Bloino, G. Zheng, J.L. Sonnenberg, M. Hada, M. Ehara, K. Toyota, R. Fukuda, J. Hasegawa, M. Ishida, T. Nakajima, Y. Honda, O. Kitao, H. Nakai, T. Vreven, J. Montgomery, J.A.J.E. Peralta, F. Ogliaro, M. Bearpark, J.J. Heyd, E. Brothers, K.N. Kudin, V.N. Staroverov, R. Kobayashi, J. Normand, K. Raghavachari, A. Rendell, J.C. Burant, S.S. Iyengar, J. Tomasi, M. Cossi, N. Rega, J.M. Millam, M. Klene, J.E. Knox, J.B. Cross, V. Bakken, C. Adamo, J. Jaramillo, R. Gomperts, R.E. Stratmann, O. Yazyev, A.J. Austin, R. Cammi, C. Pomelli, J.W. Ochterski, R.L. Martin, K. Morokuma, V.G. Zakrzewski, G.A. Voth, P. Salvador, J.J. Dannenberg, S. Dapprich, A.D. Daniels, Ö. Farkas, J.B. Foresman, J.V. Ortiz, J. Cioslowski, D.J. Fox, Gaussian 09, Revision A.02, Gaussian, Inc., Wallingford CT, 2009.
- [25] A.D. Becke, Density-functional thermochemistry 3. The role of exact exchange, *J. Chem. Phys.* 98 (1993) 5648–5652.
- [26] C.T. Lee, W.T. Yang, R.G. Parr, Development of the Colle-Salvetti correlation-energy formula into a functional of the electron-density, *Phys. Rev. B* 37 (1988) 785–789.
- [27] I.S. AGUI Program from Semichem, KS 66216, 2016. <http://www.semichem.com/>.
- [28] H.J. Chun, N. Meinander, J.R. Villarreal, J. Laane, Vibrational spectra, theoretical calculations, and two-dimensional potential energy surface for the ring-puckering vibrations of 2,4,7-trioxo[3.3.0]octane, *J. Phys. Chem. A* 119 (2015) 410–417.